Published in final edited form as:
Bioconjug Chem. 2011 December 21; 22(12): 2531–2538. doi:10.1021/bc2003617.

Activatable Optical Imaging with a Silica-Rhodamine Based Near Infrared (SiR700) Fluorophore: A comparison with cyanine based dyes

Thomas E. McCann[†], **Nobuyuki Kosaka**[†], **Yuichiro Koide**[‡], **Makoto Mitsunaga**[†], **Peter L. Choyke**[†], **Tetsuo Nagano**[‡], **Yasuteru Urano**[§], and **Hisataka Kobayashi**[†,*]

[†]Molecular imaging program, Center for Cancer Research, National Cancer Institute, National Institutes of Health, 10 Center Dr., Bethesda, MD 20892-1088, USA

[‡]Graduate School of Pharmaceutical Sciences, the University of Tokyo, 7-3-1 Hongo, Bunkyo-ku, Tokyo 113-0033, Japan

[§]Graduate School of Medicine, the University of Tokyo, 7-3-1 Hongo, Bunkyo-ku, Tokyo 113-0033, Japan

Abstract

Optical imaging is emerging as an important tool to visualize tumors. However, there are many potential choices among the available fluorophores. Optical imaging probes that emit in the visible range can image superficial tumors with high quantum yields, however, if deeper imaging is needed then near infrared (NIR) fluorophores are necessary. Most commercially available NIR fluorophores are cyanine based and are prone to non-specific binding and relatively limited photostability. Silica-containing rhodamine (SiR) fluorophores represent a new class of NIR fluorophores, which permit photoactivation via H-dimer formation as well as demonstrate improved photostability. This permits higher tumor-to-background ratios (TBRs) to be achieved over longer periods of time. Here, we compared an avidin conjugated with SiR700 (Av-SiR700) to similar compounds based on cyanine dyes (Av-Cy5.5 and Av-Alexa Fluor 680) in a mouse tumor model of ovarian cancer metastasis. We found that the Av-SiR700 probe demonstrated superior quenching enabling activation after binding-internalization to the target cell. As a result, Av-SiR700 had higher TBRs compared to Av-Cy5.5, and better biostability compared to Av-Alexa Fluor 680.

Keywords

Near infrared; molecular imaging; cancer; activatable; cyanine; rhodamine

INTRODUCTION

Target-specific optical imaging probes are promising tools in the molecular imaging of cancer. Optical imaging probes offer high sensitivity, low cost, portability, and do not entail exposure to ionizing radiation. However, optical imaging is limited by poor tissue penetration. The use of fluorophores that absorb and emit in the near infrared (NIR) range

[*]**Correspondence to:** Hisataka Kobayashi, M.D., Ph.D. Molecular Imaging Program, Center for Cancer Research, National Cancer Institute, NIH, Building 10, Room B3B69, MSC1088, Bethesda, MD 20892-1088. Phone: 301-451-4220; Fax: 301-402-3191; kobayash@mail.nih.gov.

Supporting Information Available. Analytical mass spectroscopy conditions and data of all conjugates are shown in the Supporting information. This material is available free of charge via the Internet at http://pubs.acs.org.

have less absorption and scatter from tissue, permitting deeper tissue penetration than is possible with fluorophores based on visible light. Another critical feature of an optical imaging probe is that it has high tumor-to-background ratios (TBRs). One way to achieve this is to have extremely high binding affinities for the tumor and rapid excretion of the unbound compound. Another, more practical approach, is to activate the fluorescence only upon binding to the target tissue; thus unbound conjugates yield minimal signal while target-bound conjugates have high signal leading to very high TBR. Optical imaging is unique in its ability to be activatable as opposed to radionuclide imaging that is "always on" [1, 2]. A number of quenching mechanisms have been implicated in fluorescence activation. One method is the formation of H-dimers using xanthene based fluorophores, such as rhodamine; H-dimer formation of these fluorophores leads to efficient quenching [3].

An optical probe must also be able to withstand biodegradation after internalization since this affects the durability of the signal. Rhodamine core fluorophores generally demonstrate better photostability and biostability than cyanine-based dyes and have high fluorescence quantum yield [4].

Thus the optimal imaging probe is one that is highly activatable, yet photostable and, absorbs and emits light in the NIR. While several cyanine based optical probes are commercially available, rhodamine based probes are not. Recently, Koide et al. described silica-containing rhodamine dyes (SiR), with excellent photophysical properties such as an emission peak at over 650 nm [5]. However, the ability of SiR dyes to quench via H-dimer formation *in vitro* and *in vivo*, while maintaining good *in vivo* photo- and bio-stability has not been evaluated. Here, we compare conjugates of avidin SiR fluorophore (Av-SiR700) with two cyanine-based NIR fluorophores conjugates Av-Cy5.5 and Av-Alexa Fluor 680 in a mouse model of metastatic ovarian cancer during *in vivo* optical imaging.

EXPERIMENTAL PROCEDURES

Amino-Reactive Near Infrared Fluorophores

Amino-reactive Cy5.5- and AlexaFlour680-succinimidyl esters were purchased from GE Healthcare, (Piscataway, NJ) and Invitrogen Co. (Carlsbad, CA), respectively. The synthesis method of SiR700-succinimidyl esters has been published [5, 6]. The chemical structures of all three NIR fluorophores are shown in (Fig 1).

Synthesis of Avidin-Conjugated Near Infrared Fluorophores

Avidin (6 nmol), was purchased from Pierce Biochemical, Inc. (Milwaukee, WI), and was incubated with amino-reactive NIR fluorophores (Cy5.5 and SiR700; 60 nmol, Alexa680; 40 nmol) in 0.1M phosphate buffer (pH 8.5) at room temperature for 15 min. Each mixture was purified with a Sephadex G25 column (PD-10; GE Healthcare, Piscataway, NJ). The protein concentration was determined by measuring the absorption at 280 nm with a UV-Vis system (8453 Value UV-Visible Value System; Agilent Technologies, Santa Clara, CA). The concentration of NIR fluorophores was measured by absorption with the UV-Vis system to confirm the number of fluorophore molecules conjugated to each avidin molecule [7]. The number of fluorophore molecules per all avidin conjugates was ~3.

H-dimer formation and quenching efficiency of Av-Cy5.5, Av-Alexa 680, and SiR700 in vitro

The quenching-dequenching characteristics of each avidin-conjugate were investigated by treating the conjugates with 5% SDS to disassociate any molecular interaction between fluorophores. The fluorescence signal intensity of each conjugate was measured with a fluorescence spectrometer before and after 5% SDS (Perkin-Elmer LS55, Perkin-Elmer,

Shelton, CT, USA). The absorption spectrum was measured with a UV-Vis system (8453 Value UV-Visible Value System; Agilent Technologies, Santa Clara, CA).

Cell Culture

An established ovarian cancer cell line known to overexpress the β-D-galactose receptor, SHIN3, was used for *in vitro* fluorescence microscopy, flow cytometry, and *in vivo* optical imaging using a murine intraperitoneal disseminated ovarian cancer model. The cell lines were grown in RPMI 1640 medium (Gibco, Gaithersburg, MD) containing 10% fetal bovine serum (FBS) (Gibco), 0.03% L-glutamine at 37°C, 100 units/mL penicillin, and 100 μg/mL streptomycin in 5% CO_2.

Fluorescence Microscopy

SHIN3 cells (1×10^4) were plated on a cover glass bottom culture well and incubated for 16 h. Then, Av-Cy5.5, Av-Alexa 680, or Av-SiR700 was added to the medium (3 μg/mL) and the cells were incubated for 4 h. Cells were washed three times with phosphate-buffered saline (PBS), RPMI 1640 medium was added back to all samples not imaged immediately, and fluorescence microscopy was performed immediately (T0), 24, 48, or 72 h later using an Olympus BX61 microscope (Olympus America Inc., Melville, NY) equipped with the following filters: excitation wavelength 590 to 650 nm, emission wavelength 665 to 740 nm. Transmitted light differential interference contrast (DIC) images were also acquired.

Flow Cytometry

Flow cytometry was performed to detect the *in vitro* stability of Av-Cy5.5, Av-Alexa 680, and Av-SiR700 in SHIN3 cancer cells. SHIN3 cells (1×10^4) were plated on a 6 well culture plate and incubated for 16 h. Av-Cy5.5, Av-Alexa 680, or Av-SiR700 was added to the medium (3 μg/mL) and the cells were incubated for 8 h. Next, the cells were washed three times with PBS, RPMI 1640 medium was replaced, and cells were trypsinized either immediately, 24, 48, or 72 h later. Then, flow cytometry was performed. A 635 nm red diode laser was used for excitation, and fluorescence signal from cells was collected using a 661/16 nm band-pass filter. Cells were analyzed in a FACScan cytometer (Becton Dickinson, Franklin Lakes, NJ), and all data were analyzed using CellQuest software (Becton Dickinson). *In vitro* biostability of each NIR-probe was measured as rate of change in mean fluorescence intensity (MFI) over time from 0 to 72 h.

Animal Model of Peritoneal Metastases

All procedures were carried out in compliance with the *Guide for the Care and Use of Laboratory Animal Resources* (1996), National Research Council, and approved by the institutional Animal Care and Use Committee. The tumor xenografts were established by intraperitoneal injection of 4×10^6 SHIN3 cells suspended in 200 μL of PBS in female nude mice (National Cancer Institute Animal Production Facility, Frederick, MD). Experiments with tumor-bearing mice were performed at 14–17 days after injection of the cells.

In Vivo Fluorescence Imaging

25 μg each of Av-Cy5.5, Av-Alexa 680, and Av-SiR700 were diluted in 300 μL PBS and injected into the peritoneal cavities of tumor bearing mice. Then, 4, 24, or 72 h after intraperitoneal injection, mice were euthanized with carbon dioxide inhalation. Immediately afterwards, the abdominal cavities were exposed and the 3 mice, each representing a different time point, were placed side by side on a nonfluorescent plate to compare fluorescence intensity for each NIR-probe over time. NIR fluorescence imaging was performed with the Pearl Imager (LI-COR Biosciences, Lincoln, NE). The instrument is a light-tight chamber equipped with a cooled charge-coupled device (CCD) camera.

Illumination was provided by a 685 nm diode laser, and the peak emission band is at 720 nm. Images were acquired and processed using Pearl Cam Software v1.0 (LI-COR Biosciences).

Determination of Target to Background Ratios for each NIR Probe

NIR fluorescence images of the whole abdominal cavity were obtained as described above. The TBRs of each NIR probe were determined by placing a region of interest (ROI) over tumors labeled 4 h after injection of NIR probe and an ROI of equal size over surrounding normal abdominal tissue of the same animal. ROI total signal intensity for tumors was then compared with total signal intensity from the ROI of the surrounding tissue. Image processing was performed with Pearl Cam Software v1.0 (LI-COR Biosciences).

Ex Vivo Fluorescence Imaging For Quantitation

Tumors were removed after *in vivo* imaging. Tumor explants were placed on a nonfluorescent plate and NIR imaging was performed and processed.

Semi-Quantitative Analysis of In Vivo Stability of NIR-Probes

NIR fluorescence images of the tumor explants were obtained as described above. The *in vivo* stability of each NIR probe was compared using semi-quantitative analysis. Briefly, ROIs were drawn around each tumor implant, and the average fluorescence intensity was used to quantify signal for each NIR probe at 4, 24, and 72 h after injection of NIR probe. *In vivo* stability of each NIR probe over time was determined by comparing the percent decrease in the MFI relative to the MFI measured at the 4 h time point.

Statistical Analysis

Comparison of TBR between NIR probe and *in vivo* stability for each probe over time was done using one-way ANOVA with Tukey's multiple comparisons post-test. All statistical analysis was performed using GraphPad Prism version 4.0c for Macintosh (GraphPad Software, San Diego CA, www.graphpad.com).

RESULTS

Av-SiR700 demonstrates H-dimer formation and efficient quenching in vitro

The absorbance spectra of Av-Cy5.5, Av-Alexa 680, and Av-SiR700 are displayed in (Fig 2a). A blue shifted absorbance peak representing H-dimer formation was observed for all three conjugates. The addition of SDS was used to dissociate the H-dimers. Following SDS addition, the absorption of Av-SiR700 demonstrated an increase in absorption of the monomer peak and a decrease in the blue shifted H-dimer peak. Alternatively, Av-Cy5.5 and Av-Alexa 680 demonstrated decreases in the H-dimer peak after the addition of SDS, however, there were small changes in the absorbance of the monomer peak. The amount of H-dimer formation was determined by the change in absorption of the H-dimer absorption peak relative to the monomer peak for both Av-Cy5.5, Av-Alexa 680 and Av-SiR700 before and after dissociation of H-dimers by addition of SDS as described previously [8]. The H-dimer ratios for Av-Cy5.5, Av-Alexa 680 and Av-SiR700 were 1.16, 1.29, and 2.13, respectively.

The amount of signal quenching from H-dimer formation can be appreciated by the amount of fluorescence activation observed after addition of SDS. Av-Cy5.5, Av-Alexa 680, and Av-SiR700 all demonstrate an increase in fluorescence intensity after addition of SDS (Fig 2b). The ratio of peak fluorescence intensity after SDS addition to peak fluorescence

intensity before SDS addition for Av-Cy5.5, Av-Alexa 680, and Av-SiR700 was 1.9, 1.58, and 8.35, respectively.

In vitro stability of NIR probes

Fluorescence Microscopy—After 4 h incubation with 3 μg/mL of either Av-Cy5.5, Av-Alexa 680, or Av-SiR700; live cell imaging demonstrated intracellular uptake of each imaging probe documented by discrete intracellular punctuate signals representing probe uptake by lysosomes (Fig 3). At the initial time point (T0) images of SHIN3 cells using Av-Cy5.5 and Av-Alexa 680 demonstrate high background signal due to non-specific binding of Av-Cy5.5 and Av-Alexa 680 to areas where there were no SHIN3 cells present (asterisks). Fluorescence microscopy of SHIN3 cells labeled with Av-SiR700 at T0 demonstrated specific labeling of SHIN3 cells with minimal nonspecific binding due to H-dimer formation and quenching. Serial imaging performed at 24, 48, and 72 h after washing with PBS demonstrated a progressive decrease in signal for all three NIR probes. However, Av-Cy5.5 and Av-SiR700 were brighter than Av-Alexa 680 *in vitro*, so live cell images were obtained at 200 ms for both Av-Cy5.5 and Av-SiR700, and images were obtained at 500 ms for Av-Alexa 680.

Flow cytometry

To evaluate *in vitro* NIR imaging probe stability after target binding, we performed FACS on SHIN3 cells after 8 h incubation with either Av-Cy5.5 or Av-Alexa 680, or Av-SiR700. Then, we performed serial FACS analysis at 24, 48, and 72 h after removal of each NIR imaging probe from the culture medium. The corresponding histograms are shown (Fig 4a–c). The MFI values for Av-Cy5.5, Av-Alexa 680, and Av-SiR700 were used to determine the relative decrease in fluorescence signal (Fig 4d). Time course analysis was performed expressing MFI over time as a percentage of MFI at 0 h, and MFI values decreased for each NIR fluorophore by 35.8%, 44.9%, and 31%, respectively, at 24 h. At 48 h, the decrease in MFI from MFI at 0 h for Av-Cy5.5, Av-Alexa 680, and Av-SiR700 was 67%, 75.3%, and 55.8%, respectively. After 72 h, the decrease in fluorescent intensity for each of the NIR probes from baseline was 73.7%, 80.1%, and 61.6%, respectively.

Assessment of NIR probes in vivo

To evaluate the *in vivo* characteristics of each NIR imaging probe, Av-Cy5.5, Av-Alexa 680, or Av-SiR700 were injected into the peritoneal cavities of mice with disseminated peritoneal SHIN3 ovarian cancer implants and side by side *in vivo* fluorescent images of the entire exposed abdomen were obtained at 4, 24, or 72 h after NIR imaging probe injection (Fig 5a–c). TBRs were determined by drawing an ROI over tumors and drawing an ROI of equal size over a non-tumor-bearing area adjacent to the tumor within the abdominal cavity. The TBR for each NIR imaging probe is graphically represented (Fig 5d). The average TBRs of tumors targeted with Av-Cy5.5, Av-Alexa 680, and Av-SiR700 at 4 h after administration of each imaging probe was 2.7, 3.1, and 5.2, respectively. Av-SiR700 demonstrated the highest relative TBR of the NIR imaging probes we tested, but the TBR calculated for Av-SiR700 was only statistically significantly different compared to Av-Cy5.5 ($p<0.05$).

To evaluate *in vivo* stability of each NIR imaging probe, we removed tumors labeled with each NIR imaging probe and placed them on a nonfluorescent plate. Tumor explants for each NIR imaging probe were imaged side by side to compare tumor signal at 4, 24, or 72 h after probe injection (Fig 6a). Then, an ROI was drawn around each tumor explant and average signal intensity was calculated and used to determine the decrease in signal over time for each NIR imaging probe. The time course showing the decrease of average intensity for each NIR imaging probe expressed as a percentage of fluorescence relative to the 4 h time point is illustrated in (Fig 6b). Change in average intensity relative to the 4 h time point

at 24 h for Av-Cy5.5, Av-Alexa 680, and Av-SiR700 was 114.5%, 19.3%, and 72.4%, respectively. At the 72h time point the decrease in average intensity for each NIR imaging probe as a percentage of the 4 h time point was 53.8%, 2.8%, and 42.6%, respectively. Av-Cy5.5 demonstrated less relative decrease in fluorescence when compared to Av-Alexa 680 and Av-SiR700; however, the difference observed for Av-Cy5.5 was not statistically significant relative to Av-SiR700. Interestingly, *in vivo* average fluorescence of tumors labeled with Av-Cy5.5 demonstrated a relative increase in fluorescence between 4 and 24 h after injection. Av-Alexa 680 demonstrated the lowest *in vivo* stability (compared with Av-Cy5.5 $p<0.001$ and Av-SiR700 $p<0.01$) at 72 h.

DISCUSSION

There are several key issues in optical probe design. The required tissue penetration of light needed for a specific clinical application is dependent on the wavelength of emitted light; NIR allows more depth of penetration than does visible light and results in lower autofluorescence. Another design parameter is the length of time that the fluorescence is required for an application, which is dependent on the biostability of the conjugate. Finally, the desired sensitivity of the agent is dependent on the TBR which can be improved by either increasing the binding affinity to the target or decreasing the background signal or both [9–11]. Advances in chemistry have led to the development of activateable optical imaging probes that have higher TBR when compared to “always on” fluorophores [12–14]. Several different mechanisms currently exist for the development of activateable optical imaging probes.

For instance, at high concentrations, xanthene derived fluorophores such as rhodamines form H-type and J-type homo-dimers that efficiently quench fluorescence [15–17]. H-type homo-dimers can also form at much lower concentrations after the fluorophore is covalently conjugated to proteins [3]. This homo-dimer formation induces short (H-dimer) or long (J-dimer) shifts of the fluorophore’s absorbance spectra. The presence of a blue shifted absorption peak in addition to the expected monomer absorption peak is indicative of H-dimer formation as shown in the Table 1. H-dimer absorption shifts may occur by several processes. Xanthene derived fluorophores are unique in that two identical molecules may come together to form H-homodimers with very short distances between the fluorophores. In this circumstance, the H-dimers may behave as a single quantum system that can delocalize excitation energy resulting in almost complete loss of fluorescence emission through excitation formation [15]. Once the conjugates are released from each other by changes in pH or by enzymatic processes, the fluorophores will again fluoresce. Another process by which fluorescence quenching may occur is when two fluorophores interact with each other such that they donate or accept partially excited photons from each other leading to the incoherent transfer of energy and resulting in fluorescence quenching [16]. This interaction, known as Forster resonance energy transfer (FRET), occurs at slightly larger distances up to 10 nm than H-dimer formation within 1 nm [15, 16] and results in less effective quenching. Previously, activateable NIR optical imaging probes were based on cyanine core fluorophores [18]. Activateable NIR imaging probes using cyanine cores mostly utilized FRET as a means to quench fluorescence. However, with the development of SiR fluorophores, which have xanthene-based rhodamine cores, H-dimer formation readily occurs. SiR fluorophores are able to form H-dimers, as well as undergo FRET, and can be designed to utilize the photon-induced electron transfer (PeT) effect to create activatable probes.

One method of distinguishing quenching due to H-dimer formation from FRET quenching is by chemically dissociating the H-dimers and looking for a change in the absorbance characteristics [17]. The dissociation of quenched H-dimers results in a decrease in the H-dimer absorption peak and a subsequent increase in absorption of the monomer peak.

However, molecules that are quenched primarily due to FRET, demonstrate a minimal decrease in absorbance at the H-dimer peak; but they generally do not strongly influence the absorbance at the monomer peak. Thus, the absorbance of the monomer peak remains relatively unchanged even after dequenching, although the fluorescence signal can be activated regardless of either quenching mechanism.

In this study SDS was used with the three agents, Av-SiR700, Av-Cy5.5 and Av-Alexa680, to detect changes in the absorbance characteristics of each imaging probe. Av-Cy5.5 initially demonstrated a blue shifted peak in absorbance as well as the typical peak representing the monomer. However, upon addition of SDS, there was slight increase in absorbance of the monomer peak that showed only 32% of Cy5.5 molecules formed H-type dimer. From this it can be concluded that Av-Cy5.5 fluorescence quenching is mostly caused by FRET rather than the more effective H-dimer quenching. In contrast, upon addition of SDS to Av-SiR700, the decrease in the blue shifted peak is accompanied by an increase in absorbance at the monomer peak suggesting that 80% of SiR700 molecules formed H-type dimer resulted in quenching of the SiR700 is due to the formation of H-dimers, which effectively quenched fluorescence emission up to 88%.

It must be noted that different activation and quenching strategies may act independently of one another allowing the combination of multiple quenching methods. This was recently demonstrated by using H-dimer formation in combination with a pH dependent PeT quenching in the design of an activateable optical probe. This led to an optical imaging probe that demonstrated higher TBR for tumor nodules during endoscopy than an activateable probe that utilized H-dimer formation alone [8].

Av-SiR700 demonstrated specific visualization of SHIN3 cells without nonspecific binding. However, both Av-Cy5.5 and Av-Alexa 680 had nonspecific background signals observeable by fluorescence microscopy. FACS time course analysis was used to determine if Av-SiR700 was stable after endocytosis by target cells. At all time points analyzed Av-SiR700 demonstrated less fluorophore degradation than Av-Cy5.5 and Av-Alexa 680. Av-Alexa 680 demonstrated the most rapid degradation of fluorescence emission of the three fluorophores tested.

The *in vivo* characteristics of Av-SiR700 were assessed by determining TBR and *in vivo* biostability by measuring degradation of fluorescence intensity over time. TBR analysis showed that Av-SiR700 demonstrated higher TBRs than either Av-Cy5.5 or Av-Alexa 680. *In vivo* biostability of fluorescence signal was determined by measuring the fluorescence intensity and graphing it as a ratio of fluorescence intensity at baseline. At 24 and 72 h after probe injection, Av-Cy5.5 had less deterioration of fluorescence signal than either Av-Alexa 680 or Av-SiR700. Av-Alexa 680 had the most rapid *in vivo* degradation of fluorescence intensity. Interestingly, tumor labeled with Av-Cy5.5 demonstrated higher fluorescence intensity at the 24 h time point than the 4 h time point. This may be explained by nonspecific sequestration of Av-Cy5.5 in non-target tissues with subsequent release of the imaging probe back into the circulation enabling Av-Cy5.5 continued access to the target tissue as reported with antibody-Cy5.5 conjugates in the previous study [19]. This nonspecific sequestration of Av-Cy5.5 in non-target tissue may also be due to factors such as the probe's lipophilicity, charge, or pharmacokinetic profile.

Thus, the SiR700 demonstrates several desirable features. It is a NIR fluorophore, which utilizes a rhodamine core instead of the more typical cyanine core. Because SiR700 appears to use both H-dimer and FRET mechanisms for quenching, a more dramatic TBR could be achieved than with cyanine core fluorophores, Cy5.5 or Alexa 680. Moreover, SiR700 demonstrates excellent biostability *in vivo*. Av-SiR700 was also found to have less

nonspecific binding to the tissue than Av-Cy5.5; and Av-SiR700 demonstrated superior *in vivo* fluorescence stability when compared to Av-Alexa 680. These findings suggest that SiR700, a member of a new class of NIR probes, exhibits desirable properties that could be useful for *in vivo* optical imaging.

Acknowledgments

This research was supported by the Intramural Research Program of the NIH, National Cancer Institute, Center for Cancer Research.

The research year for T.M. was made possible through the Clinical Research Training Program, a public-private partnership supported jointly by the NIH and Pfizer Inc (via a grant to the Foundation for NIH from Pfizer Inc).

References

1. Urano Y. Sensitive and selective tumor imaging with novel and highly activatable fluorescence probes. Anal Sci. 2008; 24:51–53. [PubMed: 18187849]
2. Weissleder R, Mahmood U. Molecular imaging. Radiology. 2001; 219:316–333. [PubMed: 11323453]
3. Ogawa M, Kosaka N, Choyke PL, Kobayashi H. H-type dimer formation of fluorophores: a mechanism for activatable, in vivo optical molecular imaging. ACS Chem Biol. 2009; 4:535–546. [PubMed: 19480464]
4. Bremer C, Ntziachristos V, Weissleder R. Optical-based molecular imaging: contrast agents and potential medical applications. Eur Radiol. 2003; 13:231–243. [PubMed: 12598985]
5. Koide Y, Urano Y, Hanaoka K, Terai T, Nagano T. Development of an Si-rhodamine-based far-red to near-infrared fluorescence probe selective for hypochlorous acid and its applications for biological imaging. J Am Chem Soc. 2011; 133:5680–5682. [PubMed: 21443186]
6. Koide Y, Urano Y, Hanaoka K, Terai T, Nagano T. Evolution of group 14 rhodamines as platforms for near-infrared fluorescence probes utilizing photoinduced electron transfer. ACS Chem Biol. 2011; 6:600–608. [PubMed: 21375253]
7. Ogawa M, Kosaka N, Choyke PL, Kobayashi H. Tumor-specific detection of an optically targeted antibody combined with a quencher-conjugated neutravidin "quencher-chaser": a dual "quench and chase" strategy to improve target to nontarget ratios for molecular imaging of cancer. Bioconjug Chem. 2009; 20:147–154. [PubMed: 19072537]
8. Ogawa M, Kosaka N, Regino CA, Mitsunaga M, Choyke PL, Kobayashi H. High sensitivity detection of cancer in vivo using a dual-controlled activation fluorescent imaging probe based on H-dimer formation and pH activation. Mol Biosyst. 2010; 6:888–893. [PubMed: 20567775]
9. Hama Y, Urano Y, Koyama Y, Bernardo M, Choyke PL, Kobayashi H. A comparison of the emission efficiency of four common green fluorescence dyes after internalization into cancer cells. Bioconjug Chem. 2006; 17:1426–1431. [PubMed: 17105220]
10. Kosaka N, Ogawa M, Choyke PL, Karassina N, Corona C, McDougall M, Lynch DT, Hoyt CC, Levenson RM, Los GV, Kobayashi H. In vivo stable tumor-specific painting in various colors using dehalogenase-based protein-tag fluorescent ligands. Bioconjug Chem. 2009; 20:1367–1374. [PubMed: 19514716]
11. Longmire M, Kosaka N, Ogawa M, Choyke PL, Kobayashi H. Multicolor in vivo targeted imaging to guide real-time surgery of HER2-positive micrometastases in a two-tumor coincident model of ovarian cancer. Cancer Sci. 2009; 100:1099–1104. [PubMed: 19302283]
12. Hama Y, Urano Y, Koyama Y, Gunn AJ, Choyke PL, Kobayashi H. A self-quenched galactosamine-serum albumin-rhodamineX conjugate: a "smart" fluorescent molecular imaging probe synthesized with clinically applicable material for detecting peritoneal ovarian cancer metastases. Clin Cancer Res. 2007; 13:6335–6343. [PubMed: 17975145]
13. Kobayashi H, Ogawa M, Alford R, Choyke PL, Urano Y. New strategies for fluorescent probe design in medical diagnostic imaging. Chem Rev. 2010; 110:2620–2640. [PubMed: 20000749]

14. Ogawa M, Kosaka N, Longmire MR, Urano Y, Choyke PL, Kobayashi H. Fluorophore-quencher based activatable targeted optical probes for detecting in vivo cancer metastases. Mol Pharm. 2009; 6:386–395. [PubMed: 19718793]

15. Hernando J, van der Schaaf M, van Dijk EMHP, Sauer M, García-Parajó MF, van Hulst NF. Excitonic Behavior of Rhodamine Dimers: A Single-Molecule Study. J Phys Chem A. 2003; 107:43–52.

16. Lopez Arbeloa I, Ruiz Ojeda P. Dimeric states of Rhodamine B. Chem Phys Lett. 1982; 87:556–560.

17. Kemnitz K, Yoshihara K. Entropy-driven dimerization of xanthene dyes in nonpolar solution and temperature-dependent fluorescence decay of dimers. J Phys Chem. 1991; 95:6095–6104.

18. Weissleder R, Tung CH, Mahmood U, Bogdanov A Jr. In vivo imaging of tumors with protease-activated near-infrared fluorescent probes. Nat Biotechnol. 1999; 17:375–378. [PubMed: 10207887]

19. Ogawa M, Regino CA, Choyke PL, Kobayashi H. In vivo target-specific activatable near-infrared optical labeling of humanized monoclonal antibodies. Mol Cancer Ther. 2009; 8:232–239. [PubMed: 19139133]

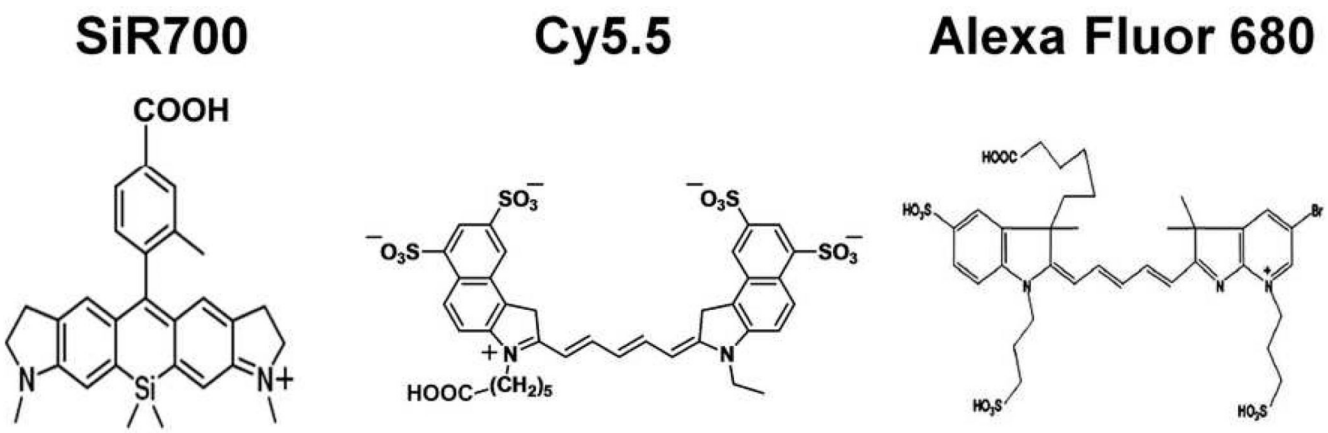

Figure 1.

Chemical structures of NIR fluorophores compared in this study. SiR700 is a NIR fluorophore synthesized on a silica rhodamine core. We compared this to two commercially available NIR fluorophores synthesized using a cyanine core, Cy5.5 and Alexa Fluor 680. Carboxyl residues are modified to succinimidyl esters and used for functionalizing fluorophores.

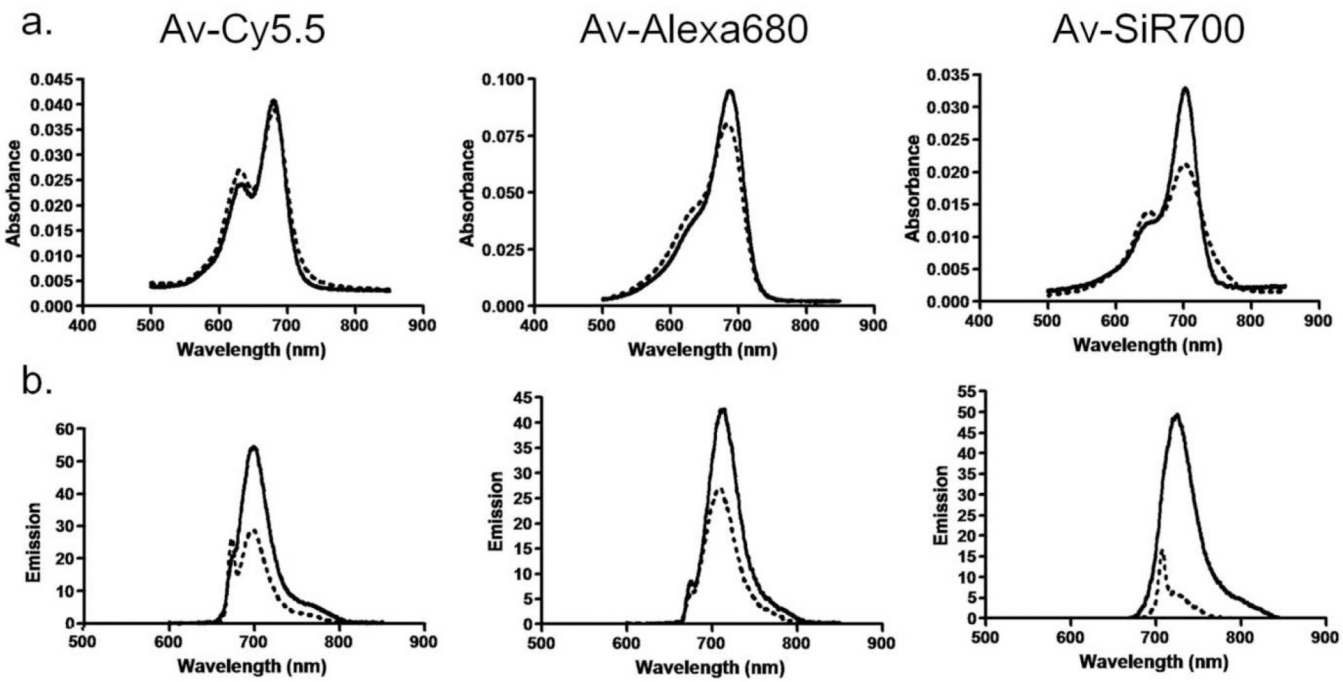

Figure 2.

(a) Absorbance spectra of NIR imaging probes, consisting of a NIR fluorophore conjugated to avidin, without SDS (dashed line) and with SDS (solid line). The blue shifted peak on the Av-Cy5.5 and Av-SiR700 curves without SDS represents H-dimer formation. Av-Alexa 680 does not demonstrate H-dimer formation. Following SDS treatment, an increase in Av-SiR700 monomer peak is characteristic of dissociation of xanthene dimers forming excitons. (b) Emission spectra of NIR imaging probes without (dashed line) and with (solid line) SDS. Emission is increased following SDS treatment for all fluorophores; however, Av-SiR700 demonstrates the greatest increase in emission following SDS.

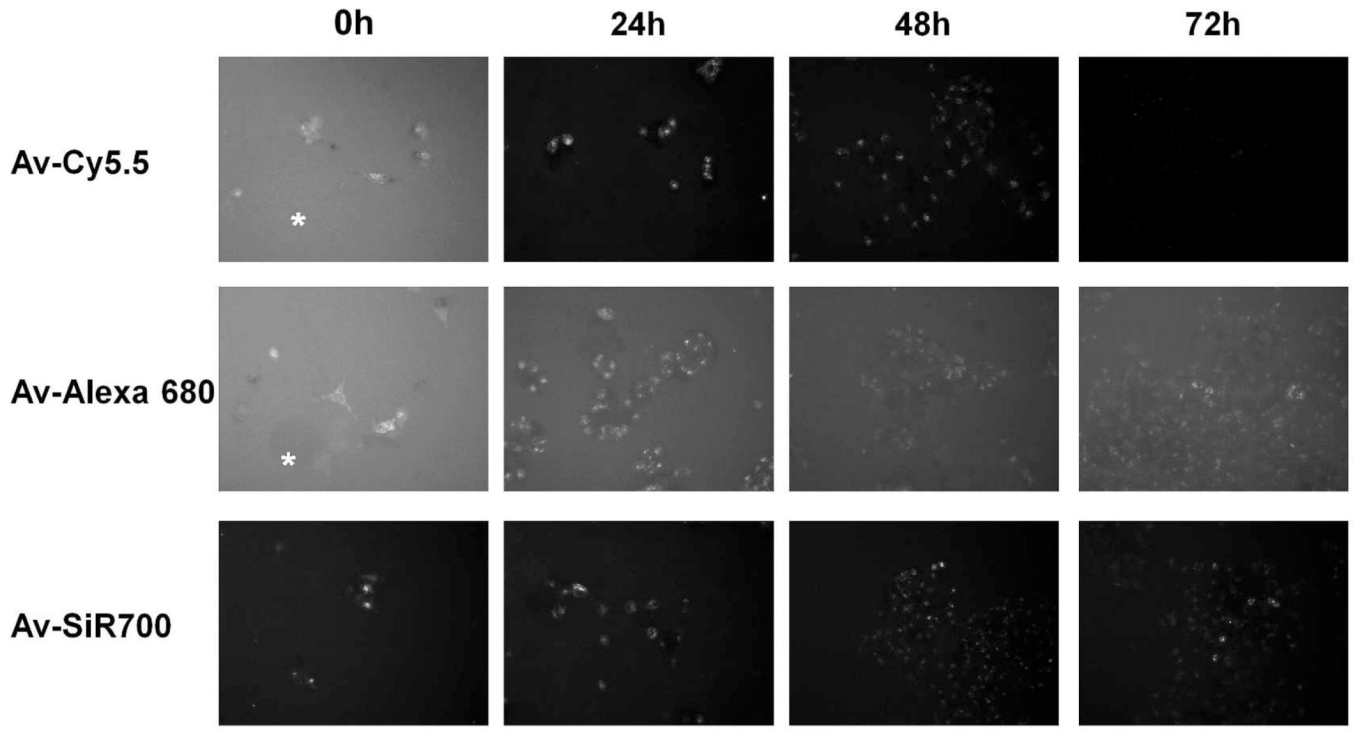

Figure 3.

Serial fluorescence microscopy images of SHIN3 cells following incubation with NIR probes. SHIN3 cells were incubated with each NIR imaging probe for 4 h and fluorescent microscopy was performed immediately (T0) and at 24, 48, and 72 h after thorough washing with PBS. At T0, SHIN3 cells could be identified after treatment with each probe, but Av-Cy5.5 and Av-Alexa 680 demonstrated considerable background signal represented by fluorescence detected where there were no cells (asterisks). 24, 48, and 72 h demonstrate a gradual decrease in fluorescent signal for each NIR probe. Exposure time: Av-Cy5.5 and Av-SiR700 =200ms, Av-Alexa 680 = 500ms.

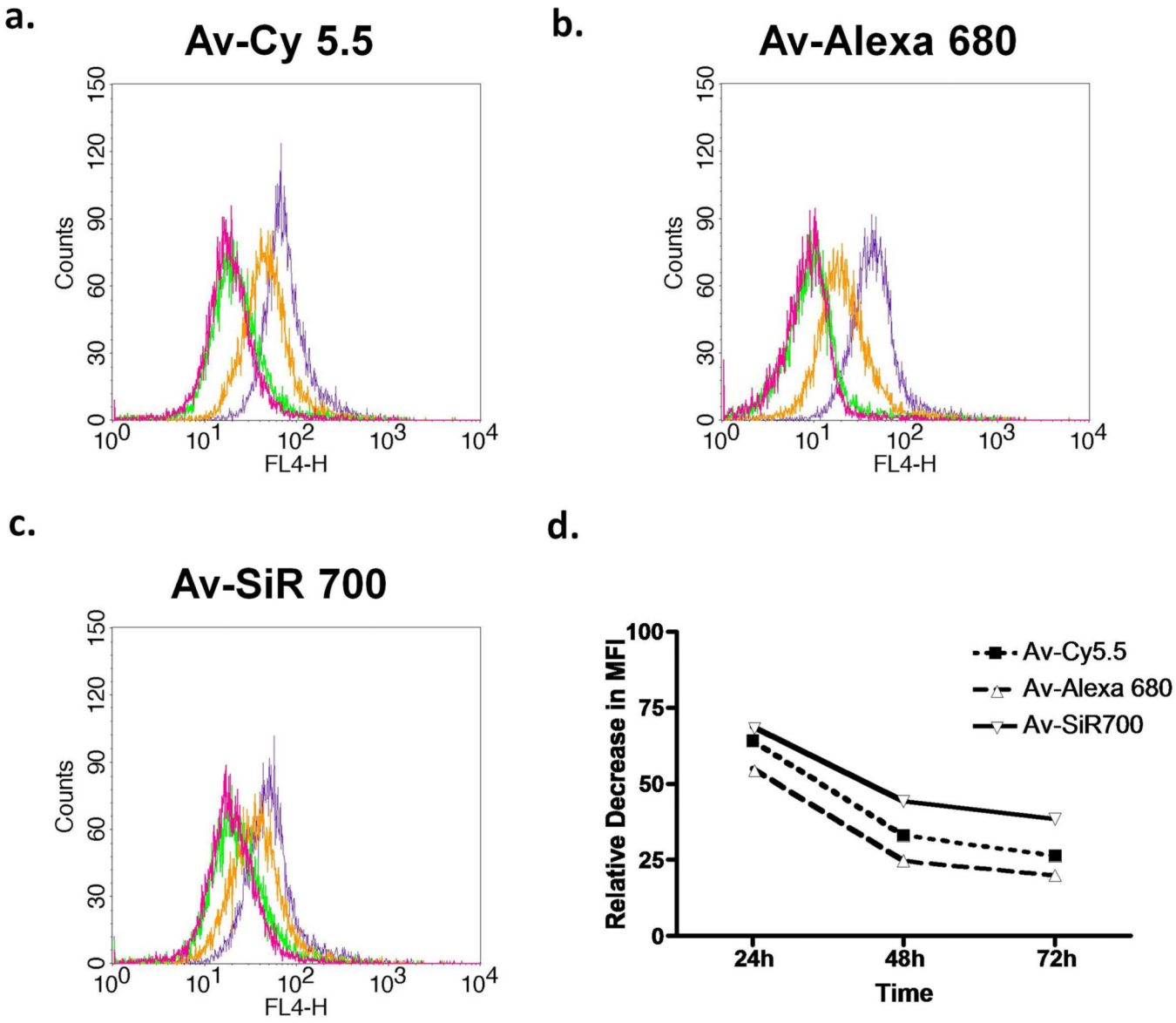

Figure 4.

Flow cytometry analysis of SHIN3 cells immediately (purple), 24 h (orange), 48 h (green), and 72 h (magenta) after PBS wash and removal of (a) Av-Cy5.5, (b) Av-Alexa 680, or (c) Av-SiR700 which demonstrates fluorescent signal degradation over time. Then, the amount of MFI degradation relative to T0 was compared (d). Av-SiR700 demonstrates less of a decrease in MFI from T0 than Av-Cy5.5 and Av-Alexa 680 at all time points.

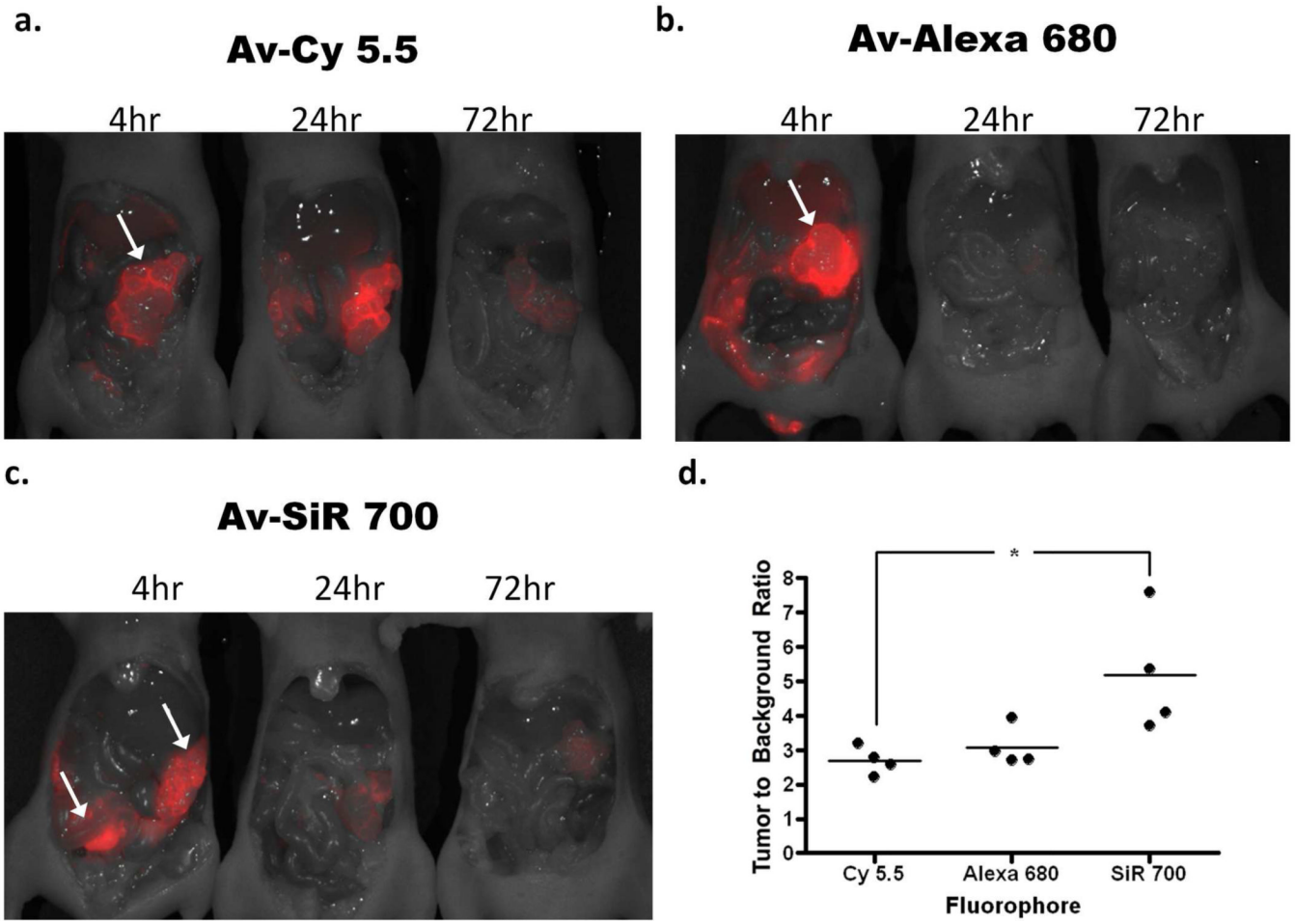

Figure 5.

In vivo fluorescence images of tumor-bearing mice 4, 24, or 72 h after intraperitoneal injection of either (a) Av-Cy5.5, (b) Av-Alexa 680, or (c) Av-SiR700. Images clearly identify SHIN3 tumors within the abdomen (arrows). Images clearly demonstrate the degradation of each NIR imaging probe over time. Interestingly, Av-Cy5.5 appears to demonstrate an increase in fluorescence intensity of tumor from 4 to 24 h after Av-Cy5.5 injection. Whole body in vivo images were then used to calculate the TBR for each NIR imaging probe at 4 h after injection. ROIs were drawn around the tumors and ROIs of the same size were drawn over the adjacent abdomen to determine background signal. This is represented graphically (d), demonstrating that Av-SiR700 has a relatively higher TBR than Av-Alexa 680, but Av-SiR700 has a significantly greater TBR than Av-Cy5.5, ($p<0.05$).

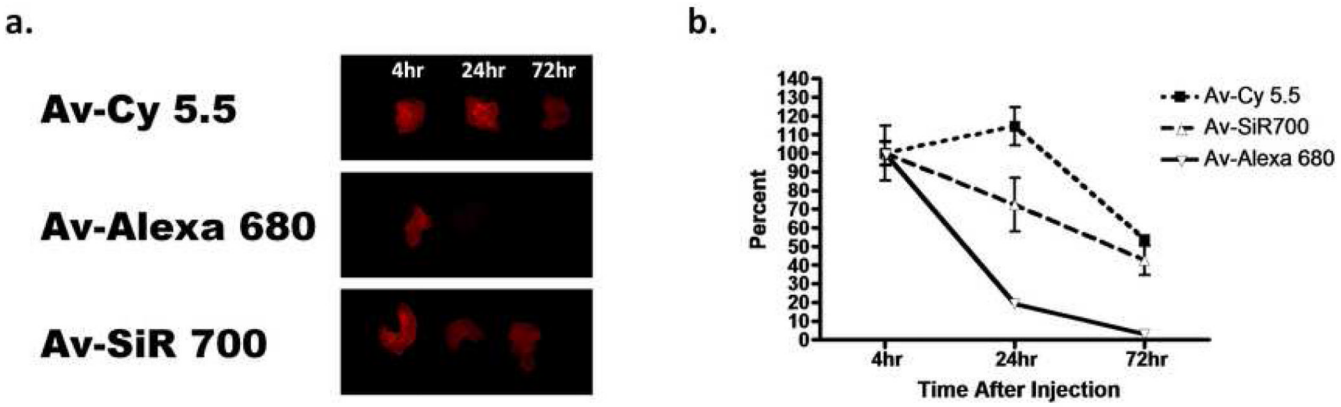

Figure 6.

(a) Tumor explants following 4, 24, or 72 h after intraperitoneal injection of either Av-Cy5.5, Av-Alexa 680, or Av-SiR700 were used to semi-quantitatively compare fluorescence intensity of each NIR imaging probe. ROIs were drawn around each tumor and average fluorescence intensity was calculated. Then, values were calculated and graphed relative to the 4 h time point. The graph demonstrating the decrease in signal for each NIR imaging probe over time is shown (b). Av-Alexa 680 demonstrates rapid decrease in fluorescence intensity with a significantly greater decrease in fluorescence intensity at 72 h than Av-Cy5.5 and Av-SiR700 with p values <0.001 and <0.01, respectively. Av-Cy5.5 demonstrates a relative increase in fluorescent intensity from 4 to 24 h but then shows a rapid decrease in fluorescence intensity. There was no significant difference in decrease in fluorescence intensity over time between Av-Cy5.5 and Av-SiR700.

Table 1

Calculated extinction coefficient values of monomer and dimer of Cy5.5, Alexa680, and SiR700 conjugated with avidin.

Reagents Forms	Av-Cy5.5		Av-Alaxa680		Av-SiR700	
	Monomer	Dimer	Monomer	Dimer	Monomer	Dimer
Peak EC at long wavelength	250000/680nm	200000/680nm	180000/687nm	86000/687nm	100000/702nm	52000/702nm
Peak EC at short wavelength	150000/629nm	210000/629nm	71000/631nm	110000/631nm	36000/647nm	47000/647nm

(EC: /cm/M)